Plasma Chem Plasma Process (2011) 31:259–271
DOI 10.1007/s11090-010-9279-7

ORIGINAL PAPER

A Comparative Study of HBr-Ar and HBr-Cl_2 Plasma Chemistries for Dry Etch Applications

Alexander Efremov · Youngkeun Kim · Hyun-Woo Lee · Kwang-Ho Kwon

Received: 8 April 2010 / Accepted: 10 December 2010 / Published online: 29 December 2010

Abstract The effects of HBr/Ar and HBr/Cl_2 mixing ratios in the ranges of 0–100% Ar or Cl_2 on plasma parameters, densities of active species influencing the dry etch mechanisms were analyzed at fixed total gas flow rate of 40 sccm, total gas pressure of 6 mTorr, input power of 700 W and bias power of 300 W. The investigation combined plasma diagnostics by Langmuir probes and the 0-dimensional plasma modeling. It was found that the dilution of HBr by Ar results in maximum effect on the ion energy flux with expected impact on the etch rate in the ion-flux-limited etch regime, while the addition of Cl_2 influences mainly the relative fluxes of Br and Cl atoms on the etched surface with expected impact on the etch rate in the reaction-rate-limited etch regime.

Keywords HBr · Cl_2 · Plasma · Dissociation · Ionization · Etch mechanism

Introduction

The binary mixtures of HBr with noble and molecular gases play an important role in the micro- and nano-electronic technology. An important feature of the binary gas mixtures is that the etch result can be optimized not only by varying the operating conditions, but also by adjusting the gas mixing ratio which directly influences the balance between chemical and physical etch pathways. Particularly, the HBr-containing plasmas are used for the dry patterning of III–V In-containing semiconductors (mainly for InP and InGaAs) in order

A. Efremov
Department of Electronic Devices and Materials Technology, State University of Chemistry and Technology, 7 F. Engels St., 153000 Ivanovo, Russia

Y. Kim · K.-H. Kwon (✉)
Department of Control and Instrumentation Engineering, Korea University, Jochiwon, Chungnam 339-700, Korea
e-mail: kwonkh@korea.ac.kr

H.-W. Lee
Division of Electronic, Computer, and Communication Engineering, Hanseo University, Chungnam 356-706, Korea

to save a nearly stoichiometric composition of the etched surface [1, 2]. Also, the HBr-containing plasmas have been successfully applied for the highly-anisotropic etching of both single crystal and poly-Si because of the negligible spontaneous reaction between Br and Si [3, 4]. And finally, the HBr-rich plasmas provide much lower (compared with the Cl-containing plasmas) etch rates of organic photoresists (PR) due to the graphitization and the cross-linking of the PR film caused by the UV ($\sim$110–210 nm) irradiation from the excited HBr molecules [5, 6]. Unfortunately, the most of existing works discuss only the effects of main operating parameters (gas pressure, input power, bias power and gas mixing ratio) on the etch rate and related characteristics while the relationships between plasma parameters, plasma composition and etch kinetic have received much less attention. This retards the development and optimization of the etch processes using the HBr-containing plasmas.

Numerical modeling is an attractive tool to analyze plasma physics and chemistry in low-pressure gas discharge plasmas. The simplest global (zero-dimensional, or 0D) models [7–9] operating with the volume-averaged plasma parameters are still in wide use to analyze the "dimension-less" effects such as general relationships between input plasma parameters, kinetics and densities of plasma active species. In our works [10, 11], we have discussed both diagnostics and modeling results for HBr and HBr/Ar plasmas order to analyze the effects influencing the steady-state densities of plasma active species. The aim of present work was the comparative model-based investigation of HBr/Ar and HBr/Cl_2 plasmas (plasma parameters, steady-state compositions and expected etch kinetics) in the reactor of given geometry under the same operating conditions. As the main variable parameter, we used the HBr/Ar and HBr/Cl_2 mixing ratios at fixed at fixed total gas flow rate, total gas pressure, input power and bias power. This was done in order to provide the consistence with our earlier works [10, 12] as well as to illustrate clearly how the addition of noble of chemical active gas influences HBr plasma parameters and kinetics of active species. Also, the topics of special interest in the HBr/Cl_2 plasma are the transition between two chemical etch pathways and the influence of possible reactive by-products on the dry etch kinetics.

Experimental and Modeling Details

Experimental Setup

The experiments were performed in planar inductively coupled plasma (ICP) reactor used in our previous works [10–12]. The plasma was excited in the cylindrical quartz chamber ($r = 16$ cm, $l = 12.8$ cm) at fixed gas flow rate (q) of 40 sccm, total gas pressure (p) of 6 mTorr, input power (W) of 700 W and bias power (W_{dc}) of 300 W ($-U_{dc} \sim 390$ V for pure HBr, $\sim$360 V for pure Cl_2 and $\sim$200 V for pure Ar plasmas) applied to the bottom electrode. The bottom electrode was made from anodized Al and, during the experiments, was covered by an oxidized Si wafer in order to provide the same recombination probabilities for Br, H and Cl atoms as ones on the reactor walls. Under the given set of experimental condition, the chemical etching of the wafer can be neglected. The HBr/Ar or HBr/Cl_2 mixing ratios were varied in the ranges of 0–100% Ar or Cl_2 by adjusting the partial flow rates of the individual gases.

Plasma diagnostics was realized with double probes (DLP2000, Plasmart Inc.), which were installed through the chamber wall-side view port. The probes were placed at 4 cm above the bottom electrode and centered in the radial direction. Each experimental point

was supported by at least five independent measurements with the accuracy not worse than 5%. Similarly with Refs. [10, 11], the electron temperature (T_e) and total positive ion density (n_+) were derived from the original I–V curves using the software supplied by the equipment manufacturer. The calculations involved Johnson and Malter's double probes theory [13] as well as the Allen-Boyd-Reynolds (ABR) approximation for the ion saturation current density [14]. Such approaches provide the agreement between the plasma diagnostics data obtained by various authors with various experimental techniques for pure Cl_2 and Ar ICPs [15–17] as well as between the measured and model-predicted plasma parameters for HBr, Cl_2 and Ar [10, 17, 18]. It was found also that, in both gas systems, the I–V curves are not sensitive to W_{dc}. Such situation corresponds to the domination of the collisional power loss over the powers dissipated through the fluxes of ions and electrons to the reactor walls.

0-Dimensional (Global) Plasma Model

To obtain the data on the densities and fluxes of plasma active species, we used a simplified 0-dimensional model with a Maxwellian electron energy distribution function (EEDF) and with the experimental data on T_e and n_+ as input parameters [11, 12]. The model used the six-component kinetic scheme (HBr/H_2/Br_2/H/Br/Ar) for neutral ground-state species in the HBr/Ar plasma as well as the nine-component kinetic scheme (HBr/Cl_2/H_2/Br_2/HCl/BrCl/H/Br/Cl) in the HBr/Cl_2 plasma. The modeling algorithm included the simultaneous solution of following equations: (1) The steady-state ($dn/dt = 0$) equations of chemical kinetics for both neutral and charged species in a general form of $R_F - R_V = (k_S + 1/\tau_R)n$, where R_F and R_V are the volume-averaged formation and decay rates in bulk plasma for a given type of species, n is their density, k_S is the first-order heterogeneous decay rate coefficient, and $\tau_R = \pi r^2 lp/q$ is the residence time. (2) The quasi-neutrality conditions for densities ($n_e + n_- = n_+$, where $n_- = n_{Br^-}$ for the HBr/Ar plasma while $n_- = n_{Br^-} + n_{Cl^-}$ for the HBr/Cl_2 plasma) and fluxes ($\Gamma_e = \Gamma_+$) of charged species on the reactor walls.

The list of processes taken into account by the model is shown in Table 1. The rate coefficients for electron impact processes R21–R26 were calculated as

$$k = (2e/m_e)^{1/2} \int_{\varepsilon th}^{\infty} f_M(\varepsilon)\sigma(\varepsilon)\sqrt{\varepsilon}d\varepsilon$$

where $f_M(\varepsilon)$ is the Maxwellian EEDF, εth is the threshold energy, and $\sigma(\varepsilon)$ is the process cross-section. The sets of cross-sections were taken from Refs. [19–22]. Since the direct experimental data on the cross-sections for R21–R23 are not available yet, these were approximated by the corresponding values for HCl [22]. The rate coefficients for atom-molecular reactions R27–R42 are from NIST Chemical Kinetics Database [23]. For the cases when the data on rate coefficients were reported in several references, the averaged values were used. For simplicity, we assumed the temperature of the neutral species (T) to be independent on HBr/Ar and HBr/Cl_2 mixing ratios and equal to 600 K. The rate coefficients for heterogeneous recombinations R46–R48 were found as $k_S = [(\Lambda^2/D) + (2r/\gamma\upsilon_T)]$ [24], where $\upsilon_T = (8\ k_B T/\pi m)^{1/2}$ is the thermal velocity, Λ is the effective diffusion length (Λ^{-2}=$(2.405/r)^2 + (\pi/l)^2$ *according to Refs.* [7] and [25]), D is the effective diffusion coefficient [8, 21], γ is the recombination probability. The neutral mean free paths needed to estimate D were taken as $\lambda_g \approx 1/(\sqrt{2}\pi d^2 N)$, where $N = p/k_B T$ is the total gas density, and d is the effective diameter of the given atom. Particularly, the values

Table 1 A simplified reaction set for the HBr/Ar and HBr/Cl_2 plasma modeling

N	Scheme	Rate coefficient, threshold energy
1	2	3
Electron-impact reactions		
R1	$HBr + e \rightarrow H + Br + e$	4.3–9.3 eV[a]
R2	$HBr + e \rightarrow Br^- + H$	–
R3	$HBr + e \rightarrow HBr^+ + 2e$	11.7 eV
R4	$Br_2 + e \rightarrow Br + Br + e$	3.0 eV[b]
R5	$Br_2 + e \rightarrow Br_2^- \rightarrow Br + Br^-$	–
R6	$Br_2 + e \rightarrow Br_2^+ + 2e$	10.6 eV
R7	$H_2 + e \rightarrow H + H + e$	8.8, 11.1 eV
R8	$H_2 + e \rightarrow H_2^+ + 2e$	15.4 eV
R9	$Br + e \rightarrow Br^+ + 2e$	11.8 eV
R10	$H + e \rightarrow H^+ + 2e$	13.6 eV
R11	$Cl_2 + e \rightarrow Cl_2^+ + 2e$	11.5 eV
R12	$Cl_2 + e \rightarrow Cl^- + Cl^+ + e$	12.0 eV
R13	$Cl_2 + e \rightarrow Cl + Cl^+ + 2e$	12.6 eV
R14	$Cl_2 + e \rightarrow Cl + Cl^-$	–
R15	$Cl_2 + e \rightarrow Cl + Cl + e$	3.0 eV[c]
R16	$Cl + e \rightarrow Cl^+ + 2e$	13.5 eV
R17	$Cl^- + e \rightarrow Cl + 2e$	3.4 eV
R18	$HCl + e \rightarrow H + Cl + e$	5.5 eV[d]
R19	$HCl + e \rightarrow Cl^- + H$	0.4 eV
R20	$HCl + e \rightarrow HCl^+ + 2e$	12.7 eV
R21	$BrCl + e \rightarrow Br + Cl + e$	5.5 eV[e]
R22	$BrCl + e \rightarrow Br^- + Cl$ and $Br + Cl^-$	0.4 eV[e]
R23	$BrCl + e \rightarrow BrCl^+ + 2e$	12.7 eV[e]
R24	$Ar + e \rightarrow Ar^+ + 2e$	15.8 eV
R25	$Ar + e \rightarrow Ar^*(^3P_0, {}^3P_1, {}^3P_2) + e$	11.55 eV
R26	$Ar + e \rightarrow Ar^* + e$	11.8–13.6 eV[f]
Atom-molecular reactions		
R27	$H + HBr \rightarrow H_2 + Br$	6.5×10^{-12} cm^3 s^{-1}
R28	$H + HCl \rightarrow H_2 + Cl$	5.0×10^{-14} cm^3 s^{-1}
R29	$H + Br_2 \rightarrow HBr + Br$	6.0×10^{-11} cm^3 s^{-1}
R30	$H + Cl_2 \rightarrow HCl + Cl$	1.0×10^{-11} cm^3 s^{-1}
R31	$H + BrCl \rightarrow HCl + Br$	5.0×10^{-12} cm^3 s^{-1}[g]
R32	$H + BrCl \rightarrow HBr + Cl$	2.0×10^{-12} cm^3 s^{-1}[g]
R33	$Cl + HBr \rightarrow HCl + Br$	6.0×10^{-12} cm^3 s^{-1}
R34	$Cl + HCl \rightarrow Cl_2 + H$	3.5×10^{-20} cm^3 s^{-1}
R35	$Cl + Br_2 \rightarrow BrCl + Cl$	1.5×10^{-10} cm^3 s^{-1}
R36	$Cl + H_2 \rightarrow HCl + H$	8.0×10^{-14} cm^3 s^{-1}
R37	$Cl + BrCl \rightarrow Cl_2 + Br$	1.5×10^{-11} cm^3 s^{-1}
R38	$Br + HBr \rightarrow Br_2 + H$	1.2×10^{-33} cm^3 s^{-1}
R39	$Br + HCl \rightarrow HBr + Cl$	1.0×10^{-15} cm^3 s^{-1}
R40	$Br + H_2 \rightarrow HBr + H$	1.0×10^{-20} cm^3 s^{-1}

Table 1 continued

N	Scheme	Rate coefficient, threshold energy
1	2	3
R41	$Br + Cl_2 \rightarrow BrCl + Cl$	5.5×10^{-17} cm^3 s^{-1}
R42	$Br + BrCl \rightarrow Br_2 + Cl$	3.3×10^{-15} cm^3 s^{-1}
Recombination of ions		
R43	$Br^- + n_+ \rightarrow$neutral products	1.0×10^{-7} cm^3 s^{-1}
R44	$Cl^- + n_+ \rightarrow$ neutral products	5.0×10^{-8} cm^3 s^{-1}
R45	$n_+ \rightarrow$ wall	υ/d_c
Recombination of neutrals		
R46	$Br_{(g)} + X_{(s)}$ (where X = H, Cl, Br) $\rightarrow BrX_{(s)} \rightarrow BrX_{(g)}$	$\gamma_{Br}\theta_X$
R47	$Cl_{(g)} + X_{(s)}$ (where X = H, Cl, Br) $\rightarrow ClX_{(s)} \rightarrow ClX_{(g)}$	$\gamma_{Cl}\theta_X$
R48	$H_{(g)} + X_{(s)}$ (where X = H, Cl, Br) $\rightarrow HX_{(s)} \rightarrow HX_{(g)}$	$\gamma_H\theta_X$

[a] Through the repulsive $a^1\Pi$ (εth = 4.3 eV), $A^3\Pi$ (εth = 6.0 eV) and $t^3\Sigma$(εth = 9.3 eV) states

[b] As for Cl_2

[c] Through the repulsive $B^3\Pi$ state

[d] Through the repulsive $A^1\Pi$ state

[e] As for HCl

[f] Includes $^1P_1$ (11.8 eV) and the rest levels the threshold energies of 13.6 eV and higher

[g] As for H + ClF

$d_{Br} = 3.02 \times 10^{-8}$ cm, $d_{Cl} = 1.78 \times 10^{-8}$ cm and $d_H = 9.20 \times 10^{-9}$ cm were used. The total recombination probability for Br atoms was taken as $\gamma_{Br} \approx 0.1$ that generally corresponds to $k_{S,Br} \approx 100$ s^{-1} measured in Ref. [26] for quartz as well as a quite close to one given in Ref. [27] ($\sim$0.075 at 350 K) for mono-Si surface in pure Br_2 gas. The value of $\gamma_{Cl} \approx 0.05$ was chosen according to our work [28] where it provided an acceptable agreement between measured and model-predicted Cl_2/X (X = Ar, He, N_2) plasma parameters in the same ICP reactor as was used for the current study. This is quite close to γ_{Cl} values derived in Refs. [29] and [30] from both Cl_2 plasma modeling and diagnostics, but by about 3 times higher than ones measured by Kota et al. [31] ($\sim$0.015 at 350 K). The last disagreement is probably due to the fact that the data of Ref. [31] relate not to the plasma region. The value of $\gamma_H \approx 0.01$ was taken from Ref. [32] for pure H_2 gas. Also, since each recombination mechanism R46–R48 consists of three parallel pathways, the partial values of corresponding probabilities were obtained as, for example, $\gamma_{Br\rightarrow BrX} = \gamma_{Br}\theta_X$, where θ_X is the fraction of surface sites covered by Br, Cl or H atoms. The values of θ_{Br}, θ_H, and θ_{Cl} were roughly estimated through the fluxes ($\Gamma = 0.25n\sqrt{8k_BT/\pi m}$) of corresponding species (for example, $\theta_{Br} \approx \Gamma_{Br}/(\Gamma_{Br} + \Gamma_H + \Gamma_{Cl})$) assuming their equal adsorption probabilities. When writing the kinetic equations for positive ions, we used $k_S = \upsilon/d_c$ where $d_c = 0.5rl/(rh_l + lh_r)$ [8, 9]. The ion Bohm velocities υ as well as the correction factors h_l and h_r for the radial and axial sheath sizes, respectively, are given by the low pressure $\lambda > (T_i/T_e)(r, l)$ diffusion theory [25]. For negative ions, we applied $k_S = 0$ due to the presence of negative charges on the reactor walls made from a dielectric material [15, 21]. Based on the analysis of the HCl plasma chemistry [33], we ignored the influence of the dissociative attachment to the vibrationally-excited HBr on the kinetics of negative ions. More modeling details can be found in Refs. [10–12]. The adequacy of the

given modeling algorithm with the given kinetic schemes is confirmed by an acceptable agreement between measured and calculated plasma parameters in pure HBr [10], pure Cl_2 [17], pure Ar [18] and Cl_2/Ar [34] ICPs.

Results and Discussion

Plasma Parameters and Composition

Plasma diagnostics by Langmuir probes showed that an increase in additive gas fractions results in slightly increasing electron temperatures in both HBr/Ar and HBr/Cl_2 plasmas (T_e = 3.15–3.67 eV for 0–100% Ar and 3.15–3.36 eV for 0–100% Cl_2). Corresponding data are represented in Fig. 1a. The behavior of T_e can be easily understood from the analysis of threshold energies and cross-sections for plasma components. From Table 1

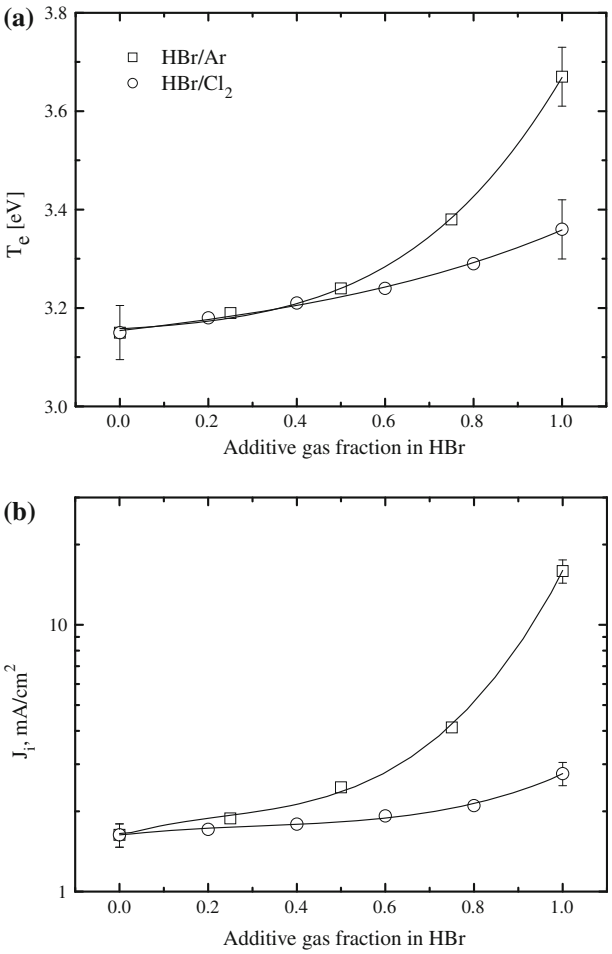

Fig. 1 Measured electron temperature (**a**) and ion current density (**b**) as functions of HBr/Ar and HBr/Cl_2 mixing ratios. The *solid lines* are to guide the eye only

and Refs. [19–22], it can be seen that the electron impact reactions for Ar have higher thresholds with closer values of excitation and ionization potentials, but lower cross-sections corresponding to the medium part of the EEDF. That is why the dilution of HBr by Ar lowers the electron energy loss in the medium part of the EEDF ($\varepsilon_{col} \approx \sum_i \sum_j y_i k_{i,j} \varepsilon_{i,j}^{th} = 1.65 \times 10^{-8} - 1.40 \times 10^{-8}$ eVcm^3/s, where y is the mole fraction for the i-type plasma component while k and εth are the rate coefficient and the threshold energy for the j-type inelastic process) and shifts T_e toward higher values. Similar results have been repeatedly reported for the Cl_2/Ar plasmas [34, 35]. In the HBr/Cl_2 plasma, the same effect is due to the high dissociation degree of Cl_2 molecules that provides $n_{Cl}/n_{Cl_2} > 3$ and $\varepsilon_{col} = 1.65 \times 10^{-8}$–$1.57 \times 10^{-8}$ eVcm^3 s^{-1} because the EEDF is noticeably influenced by the Cl-e collisions. Since for most of R1–R26 the condition εth $\geq T_e$ takes place, the corresponding rate coefficients are sensitive to the change in the additive gas fractions in both HBr/Ar and HBr/Cl_2 gas mixtures and follow the behavior of T_e (for example, $k_3 = 8.42 \times 10^{-10}$–$1.65 \times 10^{-9}$ cm^3 s^{-1} for 0–100% Ar and 8.42×10^{-10}–1.39×10^{-9} cm^3 s^{-1} for 0–100% Cl_2). However, for the threshold-less R2, R5 and R14 an increase in T_e results in decreasing rate coefficients (for example, $k_2 = 2.69 \times 10^{-10}$–$2.17 \times 10^{-10}$ cm^3 s^{-1} for 0–100% Ar and 2.69×10^{-10}–2.46×10^{-10} cm^3 s^{-1} for 0–100% Cl_2) because of decreasing fraction of low-energy electrons in EEDF.

It was found that an increase in the additive gas fraction results in increasing ion current density (1.63–15.90 mA cm^{-2} for 0–100% Ar and 1.63–2.80 mA cm^{-2} for 0–100% Cl_2, see Fig. 1b) which is associated with the similar trends for both total flux of positive ions $\Gamma_+ \approx h_l \sum n_{+,j} v_j$ (1.02×10^{16}–9.96×10^{16} cm^{-2} s^{-1} for 0–100% Ar and 1.02×10^{16}–1.75×10^{16} cm^{-2} s^{-1} for 0–100% Cl_2) and total density of positive ions (Fig. 2a). The model-predicted n_e also increases and occupies the ranges of 3.81×10^{10}–5.47×10^{11} cm^{-3} for 0–100% Ar and 3.81×10^{10}–7.22×10^{10} cm^{-3} for 0–100% Cl_2. Physically, this is supported by increasing effective ionization frequency ($\nu_{iZ} = \sum k_{iZ,j} n_j = 4.88 \times 10^4 - 6.26 \times 10^4$ s^{-1} for 0–100% Ar and 4.88×10^4–1.26×10^5 s^{-1} for 0–100% Cl_2, where $k_{iZ,j}$ and n_j are the ionization rate coefficient and the density of a j-type plasma component) as well as by the decreasing ion decay frequencies in R43 and R44. The lower n_+ and n_e values in the Cl_2-rich plasmas compared with Ar-rich plasmas are because of higher electronegativity of the first one. The dominant positive ions in pure HBr plasma are HBr^+ ($n_{HBr^+}/n_+ = 0.47$), Br_2^+ ($n_{Br_2^+}/n_+ = 0.22$) and Br^+ ($n_{Br^+}/n_+ = 0.30$). Such situation generally corresponds to the composition of neutral species with accounting for the high ionization rate coefficient for Br_2 ($k_6/k_3 = 1.9$ and $k_6/k_9 = 1.8$). The very low densities of H_2^+ ($n_{H_2^+}/n_+ = 1.91 \times 10^{-3}$) and H^+ ($n_{H^+}/n_+ = 2.73 \times 10^{-3}$) result from low ionization rates for both H_2 and H (high thresholds, low cross-sections) as well as from fast decay of these ions (low ion mass, high ion Bohm velocity). The specific feature of the HBr/Ar plasma is that the total density of HBr^+, Br^+ and Br_2^+ is higher than that for Ar^+ even if the fraction of Ar exceeds 70% (for example, $(n_{HBr^+} + n_{Br^+} + n_{Br_2^+})/n_{Ar^+} = 1.29$ for 75% Ar). This is also due to the low ionization rates for Ar atoms. Oppositely, the ionization rate coefficients for both Cl_2 and Cl are close to those for HBr, Br_2 and Br. That is why, in the HBr/Cl_2 plasma, the Cl_2^+ and Cl^+ ions begin to dominate over the HBr-related ions when the Cl_2 mixing ratio exceeds 50–55%. In pure Cl_2 plasma, the condition $n_{Cl_2^+}/n_{Cl^+} = 1.12$ takes place because the higher density of Cl^+ is suppressed by higher ion Bohm velocity and lower ionization rate coefficient for Cl atoms.

The density of negative ions generally follows the change of total attachment rate determined by $R_2 + R_5$ for HBr/Ar plasma and by $R_2 + R_5 + R_{14}$ for HBr/Cl_2 plasma. As

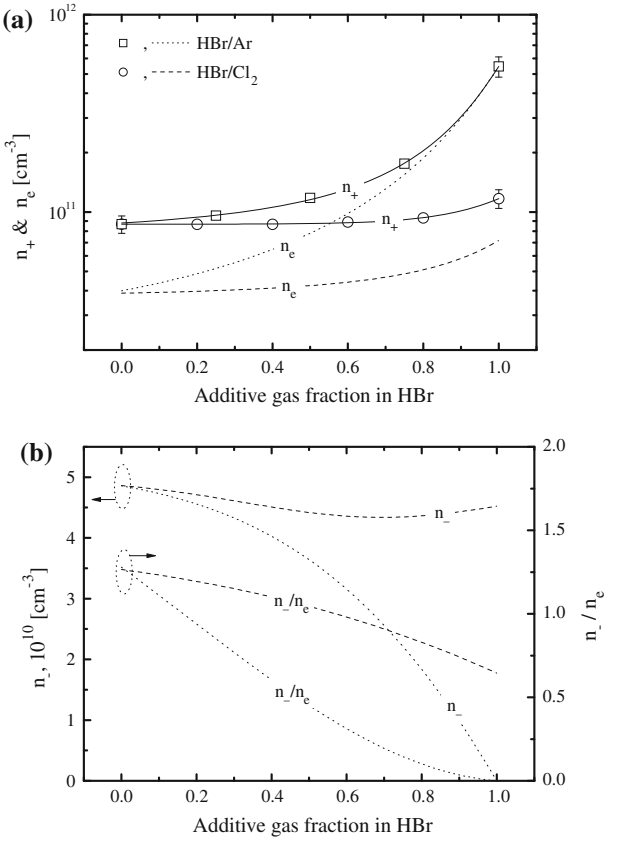

Fig. 2 Measured (*symbol* + *solid line*) and model-predicted (*dashed line*) densities of charged species as functions of HBr/Ar and HBr/Cl_2 mixing ratios

the Ar mixing ratio increases, the density of Br^- decreases monotonically in the range of 4.87×10^{10}–2.20×10^{10} cm^{-3} for 0–75% Ar (that corresponds to $n_{Br^-}/n_e = 1.28 - 0.14$) and falls down to zero at 100% Ar. As the Cl_2 mixing ratio changes from 0 to 100%, the total density of negative ions $n_- = n_{Br^-} + n_{Cl^-}$ decreases slightly in the range of 4.87×10^{10}–4.55×10^{10} cm^{-3}. The reason is that the higher dissociative attachment rate coefficient for Cl_2 ($\sim 3.6 \times 10^{-10}$ and $\sim 2.6 \times 10^{-10}$ cm^3 s^{-1} for R14 and R2, respectively) is overcompensated by higher Cl_2 dissociation degree, so that the effective attachment frequency $\nu_{att} \approx k_2 n_{HBr} + k_{14} n_{Cl_2}$ decreases from 1.0×10^4–7.5×10^3 s^{-1} for 0–100% Cl_2. Accordingly, a decrease in the relative density of negative ions n_-/n_e in the range of 1.28–0.63 takes place. The values of n_-/n_e obtained in this work are in good agreement with earlier published data for low-pressure electronegative plasmas [8, 34–36].

Figure 3 represents the influence of gas mixing ratio on the steady-state densities of neutral species in the HBr/Ar and HBr/Cl_2 plasmas. In pure HBr plasma, the dominant formation mechanism for Br atoms are R1 and R4 while the contributions of dissociative attachments R2 and R5 are much lower due to lower cross-sections that provides $k_1/k_2 = 4.6$ and $k_4/k_5 = 56$. The higher formation rate of Br atoms by electron impacts compared with that for H ($k_4/k_7 = 12.1$ and $R_1 + R_4 > R_1 + R_7$ by 2.13 times) as well as the faster decay of H atoms due to the atom-molecular reactions R27 and R29 ($(R_{27} + R_{29})/R_{48} = 2.3$) create the disproportion between Br and H densities with $n_{Br}/n_H = 8.89$. Also, since R27 and R29 additionally produce H_2 and HBr, we obtain a

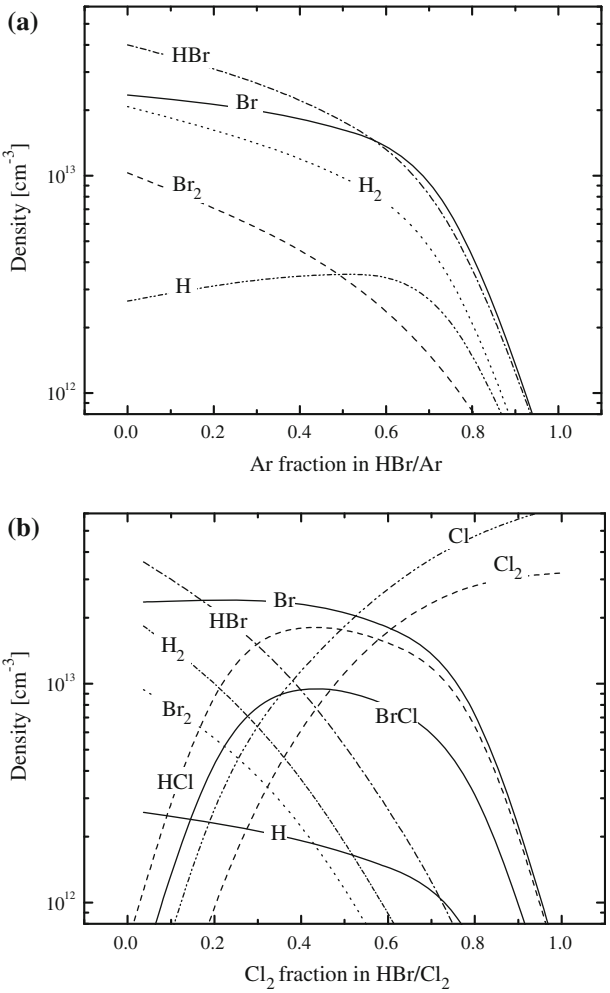

Fig. 3 Model-predicted densities of neutral ground-state species as functions of HBr/Ar and HBr/Cl_2 mixing ratios

relatively high densities of H_2 compared with those for Br_2 ($n_{Br_2}/n_{H_2} = 0.51$) as well as the relatively low dissociation degree of HBr ($n_{HBr}/(n_H + n_{Br}) = 1.7$). Similar effects were mentioned in Ref. [25] for the HCl plasma. It is important to note that an evident domination of $R_{27} + R_{29}$ over R_{48} results in a very weak sensitivity of the H atom balance to γ_H. At the same time, the contribution of R38 and R40 to the total decay rate of Br atoms is negligibly small compared with $R_1 + R_4$, so that the balance of Br atoms seems to be sensitive to γ_{Br}. However, this sensitivity is much weaker than it can be expected from the simple relation $n_{Br} \sim k_1 n_e n_{HBr}/k_{S,Br}$, and the twofold increase in γ_{Br} results only in a 1.2 times decrease in n_{Br}. This is because an increase in Br atom loss rate is partially compensated increasing Br atom formation rate in R27 and R29 because of increasing Br_2 and HBr densities. Therefore, some uncertainty in γ_H and γ_{Br} is not a critical issue influencing the overall accuracy of the model.

As the HBr/Ar mixing ratio changes toward the Ar-rich plasmas, the density of Br atoms decrease monotonically, but the condition $n_{Br} > n_{HBr}$ takes place for more than 50% Ar. This results from an increase in the dissociative collision frequency for electrons $\nu_{dis} \approx (k_1 + k_4)n_e = 497$–$866$ for 0–75% Ar and thus, in the HBr dissociation degree. The influence of metastable atoms $Ar(^3P_{0,1,2})$ on the HBr dissociation kinetics by the reaction $HBr + Ar(^3P_{0,1,2}) \rightarrow H + Br + Ar$ can be neglected. The reason is low excitation rate coefficient of $Ar(^3P_{0,1,2})$ ($k_{25} = 2.49 \times 10^{-10}$–$5.08 \times 10^{-10}$ cm^3 s^{-1} for 0–100% Ar) that produces low formation rate for metastable Ar atoms. As a result, even if the fraction of Ar reaches 80%, the condition $R_1/R_{25} \sim 3.5$ takes place while the real contribution of stepwise dissociation is much lower due to the fast heterogeneous decay of $Ar(^3P_{0,1,2})$. The same conclusions can be obtained for the stepwise dissociations of both Br_2 and H_2 molecules. The non-monotonic behavior of n_H (due to the fast decrease of their decay rate in R27 and R29) lowers the gap between Br and H atom densities and causes a decrease in both n_{Br}/n_H (8.87–3.23 for 0–75% Ar) and n_{Br_2}/n_{H_2} (0.51–0.26 for 0–75% Ar) ratios.

An increase in the Cl_2 mixing ratio in the HBr/Cl_2 plasma causes an increasing Br atom formation rate through both R33 and R35 (5.8×10^{14} cm^{-3} s^{-1} for R33 and 2.5×10^{15} cm^{-3} s^{-1} for R35 compared with 1.7×10^{15} cm^{-3} s^{-1} for R1 at 20% Cl_2). This results in the fast decay of Cl, HBr and Br_2 as well as in the accumulation of HCl and BrCl in a gas phase. Accordingly, at 20–80% Cl_2, reactions R31 and R37 also represent an essential source of Br atoms while the Br atom density keeps a constant value up to 40% Cl_2 and decreases only by 1.3 times compared with pure HBr plasma when the Cl_2 fraction reaches 60%. High electron impact dissociation rate for Cl_2 ($k_{15} = 1.12 \times 10^{-8}$–$1.23 \times 10^{-8}$ cm^3 s^{-1} compared with $k_1 = 1.72 \times 10^{-9}$–$1.98 \times 10^{-9}$ cm^3 s^{-1} for 0–100% Cl_2 due to higher dissociation cross-section and lower threshold energy) not only maintains high rates of R33, R35 and R37 in the HBr-rich plasmas, but also provides the domination of Cl atoms in the Cl_2-rich plasmas with $n_{Cl}/n_{Cl_2} = 1.5 - 3.5$ for 60–100% Cl_2. The last result is in good agreement with earlier published works on both diagnostics and modeling of Cl_2-based ICPs [26, 28]. In addition, since in the HBr-rich plasmas the decay of Cl atoms is noticeably contributed by R33 and R35 (for example, $k_{33}n_{HBr} + k_{35}n_{Br_2} = 360\,s^{-1}$ versus $k_{47} = 450$ s^{-1} for 40% Cl_2), the sensitivity of modeling results to γ_{Cl} is rather low up to 60–70% Cl_2 in HBr/Cl_2 gas mixture. That is why, the reasonable uncertainty in γ_{Cl} does not distort the basic kinetic effects determining the neutral plasma composition.

Dry Etch Kinetics

In order to analyze the possible influence of gas mixing ratio on the rate of ion-assisted chemical reaction, let's refer to the relationships given by the theory of free surface sites (Langmuir–Hinshelwood theory) [4, 37–40]. For the ion-flux-limited etch regime ($\theta \approx 1$, where θ is the fraction of the surface covered by the reaction products), the rate of physical etch pathway R_{ph} follows the parameter $Y_S\Gamma_+$, where Y_S is the sputtering yield or the yield of ion-stimulated desorption. Assuming that Y_S is proportional to the momentum transferred from the incident ion to the etched surface [4, 40], the relative behavior of R_{ph} can be simply characterized by $m_i\varepsilon^{1/2}\Gamma_+$, where m_i is the effective ion mass, and ε is the incident ion energy determined by the sum of floating potential and the negative *dc* bias voltage $-U_{dc}$ applied to the substrate. As can be seen from Fig. 4, the HBr/Ar plasma is characterized by deeper decrease in the negative *dc* bias voltage ($-U_{dc} = 395$–195 V for 0–100% Ar vs. 395–357 V for 0–100% Cl_2) and thus, in ion bombardment energy

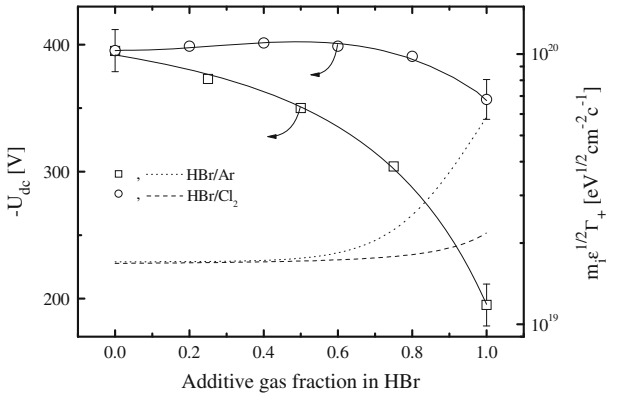

Fig. 4 Measured negative *dc* bias voltage $-U_{dc}$ (*symbol* + *solid line*) and model-predicted parameter $m_i\varepsilon^{1/2}\Gamma_+$ (*dashed line*) characterizing the ion energy flux as functions of HBr/Ar and HBr/Cl_2 mixing ratios

(ε = 415–217 eV for 0–100% Ar vs. 415–377 eV for 0–100% Cl_2) with increasing fraction of additive gas. Together with lower effective ion mass for Ar-rich plasmas than that for Cl_2-rich plasmas, this lowers the differences between ion fluxes (as was mentioned by Fig. 1b for J_i) and provides the very close values of $m_i\varepsilon^{1/2}\Gamma_+$ up to 50–60% Ar or Cl_2. However, the ion energy flux in pure Ar plasma is more than 3 times higher than that for pure Cl_2 plasma. Accordingly, the same differences in R_{ph} are expected in these systems.

For the reaction-rate-limited etch regime ($\theta \approx 0$), the steady-state rate of etch process R_{ch} (in fact, the flux of reaction products leaving the surface) can be characterized by the parameter $\sum \gamma_{R,i}\Gamma_i$, where γ_R is the reaction probability for the *i*-type neutral species, and $\Gamma \approx 0.25n\sqrt{8k_BT/\pi m}$ is their flux. Thought the condition $n_{Br} > n_H$ takes place for the HBr/Ar plasma, the fluxes of these species are quite close (2.5×10^{17}–1.17×10^{17} cm^{-2} s^{-1} for Br and 1.70×10^{17}–2.16×10^{17} cm^{-2} s^{-1} for H at 0–75% Ar) because the lower density of H atoms is overcompensated by higher thermal velocity due to the lower mass. Therefore, the equation $R_{ch} \approx \gamma_{R,Br}\Gamma_{Br} + \gamma_{R,H}\Gamma_H$ can be basically assumed. From Fig. 5a, it can be seen that, for the given Γ_{Br} and Γ_H, the relative behavior of the etch rate depends strongly on the $\gamma_{R,Br}/\gamma_{R,H}$ ratio. Particularly, for $\gamma_{R,Br}/\gamma_{R,H} < 0.1$ and $\gamma_{R,Br}\Gamma_{Br} \ll \gamma_{R,H}\Gamma_H$, the etch rate follows Γ_H and exhibits the non-monotonic behavior with an increase in Ar mixing ratio. Oppositely, for $\gamma_{R,Br}/\gamma_{R,H} > 10$ and $\gamma_{R,Br}\Gamma_{Br} \gg \gamma_{R,H}\Gamma_H$, the variation of R_{ch} correlates mainly with Γ_{Br} showing a monotonic decrease toward Ar-rich plasmas. In our opinion, the last case looks more expectable taking into account the much higher reactivity of Br atoms for the most of inorganic materials (metals, semiconductors and their oxides) used in the microelectronic technology. For the HBr/Cl_2 plasma, the case of the primary interest is the concurrence between the chemical etch pathways with Br and Cl atoms, where $R_{ch} \approx \gamma_{R,Br}\Gamma_{Br} + \gamma_{R,Cl}\Gamma_{Cl}$. As it can be seen from Fig. 5b, the condition $\gamma_{R,Br}/\gamma_{R,Cl} < 0.1$ (that means, in fact, the much lower sticking coefficient for Br atoms and/or much lower volatility for the Br-containing reaction products) provides the monotonic increase in the etch rate $R_{ch} \approx \gamma_{R,Cl}\Gamma_{Cl}$ with increasing Cl_2 fraction in the HBr/Cl_2 plasma by more than the order of magnitude. The value $\gamma_{R,Br}/\gamma_{R,Cl} \sim$ 5–7 equalizes the differences between Γ_{Br} and Γ_{Cl} that results in near-to-constant R_{ch} in both pure HBr and Cl_2 plasmas while the absolute domination of $\gamma_{R,Br}\Gamma_{Br}$ is obtained only with $\gamma_{R,Br}/\gamma_{R,Cl} > 50$. Finally, we would like to note that the dependencies shown in Fig. 5b can be disturbed by some chemical effects from the HCl molecules. These can be either the activation of the etched surface resulting in the

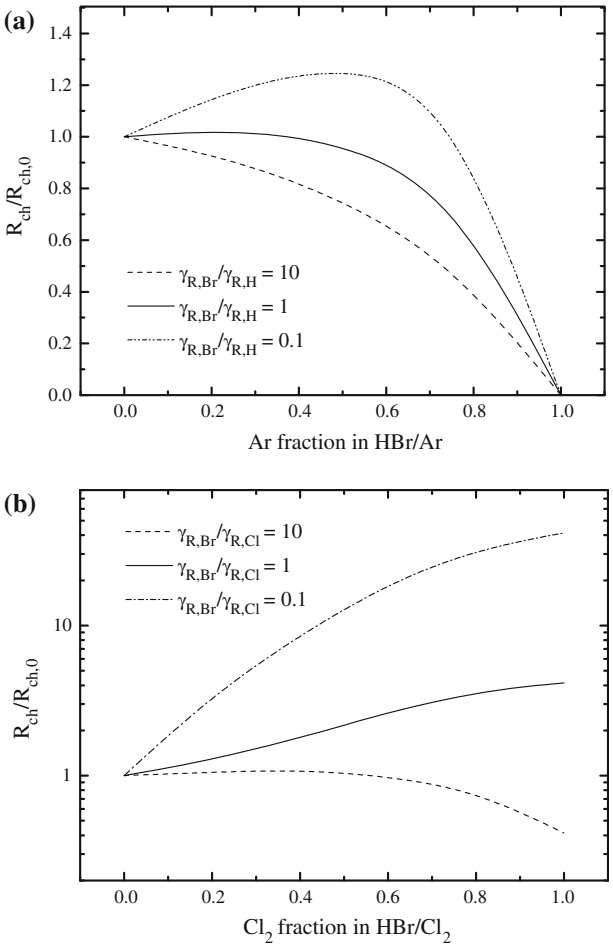

Fig. 5 Model-predicted relative changes of chemical etch rate ($R_{ch}/R_{ch,0}$, where $R_{ch,0}$ corresponds to pure HBr plasma) as functions of HBr/Ar and HBr/Cl_2 mixing ratios with different ratios of reaction probabilities for Br, H and Cl atoms

non-monotonic γ_R as follows from the changes of HCl density and flux or the direct participation of HCl molecules in the etch process.

Conclusion

In this work, we investigated the effects of HBr/Ar and HBr/Cl_2 mixing ratios on basic plasma parameters influencing the dry etch mechanisms. The investigation included plasma diagnostics by Langmuir probes aimed at obtaining electron temperature, ion current density and the total positive ion density as well as the 0-dimensional plasma modeling in order to analyze the kinetics, densities and fluxes of plasma active species. Both diagnostics and modeling were performed at fixed total gas flow rate, total gas pressure, input power and bias power. It was found that the dilution of HBr by Ar provides

the maximum change in the ion energy flux and thus, in the rate of ion-assisted chemical reaction in the ion-flux-limited etch regime. The addition of Cl_2 influences mainly the reaction-rate-limited etch regime through the Br atoms formation kinetic as well as through the concurrence of two etch pathways providing by Br and Cl atoms.

Acknowledgment This work was supported by a Korea University Grant.

References

1. Pearton SJ, Chakrabarti UK, Lane E, Perley AP, Abernathy CR, Hobson WS, Jones KS (1992) J Electrochem Soc 139:856
2. Kuo Y, Tai TL (1998) J Electrochem Soc 145:4313
3. Bestwick TD, Oehrlane GS (1990) J Vac Sci Technol A 8:1696
4. Jin W, Vitale SA, Sawin HH (2002) J Vac Sci Technol A 20:2106
5. Bazin A, Pargon E, Mellhaoui X, Perret D, Mortini B, Joubert O (2008) Advances in resist materials and processing technology XXV. In: Henderson CL (ed) Proceedings of the SPIE. 6923, p 692337
6. Pargon E, Menguelti K, Martin M, Bazin A, Chaix-Pluchery O, Sourd C, Derrough S, Lill T, Joubert O (2009) J Appl Phys 105:094902
7. Lee C, Lieberman MA (1995) J Vac Sci Technol A 13:368
8. Ashida S, Lieberman MA (1997) Jpn J Appl Phys 36:854
9. Lieberman MA, Ashida S (1996) Plasma Sources Sci Technol 5:145
10. Efremov A, Choi B-G, Nahm S, Lee HW, Min N-K, Kwon K-H (2008) J Korean Phys Soc 52:48
11. Lee HW, Kim M, Min N-K, Efremov A, Lee C-W, Kwon K-H, Jpn J (2008) Appl Phys 47:6917
12. Kim M, Min N-K, Yun SJ, Lee HW, Efremov A, Kwon K-H (2008) Microelectron Eng 85:348
13. Johnson EO, Malter L (1950) Phys Rev 80:58
14. Sugavara M (1998) Plasma etching. Fundamentals and applications. Oxford University Press Inc., New York
15. Ullal SJ, Godfrey AR, Edelberg E, Braly L, Vahedy V, Aydil ES (2002) J Vac Sci Technol A 20:43
16. Malyshev MV, Donnelly VM (2000) J Appl Phys 87:1642
17. Hopwood J, Guarnieri CR, Whitehair SJ, Cuomo JJ (1993) J Vac Sci Technol A 11:152
18. Efremov AM, Kim G-H, Kim J-G, Kim C-I (2007) Thin Solid Films 515:5395
19. Šašić O, Dujko S, Petrović Z (2007) Jpn J Appl Phys 46:3560
20. Kurepa MV, Babic DS, Belic DS (1981) J Phys B At Mol Phys 14:375
21. Gudmundsson JT (2001) Plasma Sources Sci Technol 10:76
22. Morgan WL (1992) Plasma Chem Plasma Proc 12:449
23. NIST chemical kinetica database. (2010) http://kinetics.nist.gov/kinetics/
24. Chantry PJ (1987) J Appl Phys 62:1141
25. Lieberman MA, Lichtenberg AJ (1994) Principles of plasma discharges and materials processing. Wiley, New York
26. Dzotsenidze Z, Petviashvili D, Museridze M, Sulaberidze K (2001) Bull Ga Acad Sci 164
27. Serdyuk NK, Gutorov VV, Panfilov VN (1981) React Kinet Catal Lett 16:393
28. Efremov A, Min N-K, Choi B-G, Baek K-H, Kwon K-H (2008) J Electrochem Soc 155:D777
29. Corr CS, Despiau-Pujo E, Chabert P, Graham WG, Marro FG, Graves DB (2008) J Phys D Appl Phys 41:185202
30. Curley GA, Gatilova L, Guilet S, Bouchoule S, Gogna GS, Sirse N, Karkari S, Booth JP (2010) J Vac Sci Technol. A 28:360
31. Kota GP, Coburn JW, Graves DB (1998) J Vac Sci Technol A 16:270
32. Wood BJ, Wise H (1961) J Phys Chem 65:1976
33. Efremov AM, Kim GH, Balashov DI, Kim C-I (2006) Vacuum 81:244
34. Efremov AM, Kim GH, Kim JG, Bogomolov AV, Kim CI (2007) Microelectron Eng 84:136
35. Fuller NCM, Donnelly VM, Herman IP (2002) J Vac Sci Technol A 20:170
36. Fuller NCM, Herman IP, Donnelly VM (2001) J Appl Phys 90:3182
37. Gray DC, Tepermeister I, Sawin HH (1993) J Vac Sci Technol B 11:1243
38. Winters HW, Coburn JW (1992) Surf Sci Rep 14:162
39. Lee C, Graves DB, Lieberman MA (1996) Plasma Chem Plasma Process 16:99
40. Efremov AM, Kim DP, Kim C-I (2004) IEEE Trans Plasma Sci 32:1344